Published in final edited form as:
Int J Radiat Oncol Biol Phys. 2014 November 15; 90(4): 952–958. doi:10.1016/j.ijrobp.2014.07.028.

Is Diaphragm Motion a Good Surrogate for Liver Tumor Motion?

Juan Yang, MS[*,†], **Jing Cai, PhD**[*], **Hongjun Wang, PhD**[†], **Zheng Chang, PhD**[*], **Brian G. Czito, MD**[*], **Mustafa R. Bashir, MD**[‡], **Manisha Palta, MD**[*], and **Fang-Fang Yin, PhD**[*]

[*]Department of Radiation Oncology, Duke University Medical Center, Durham, North Carolina

[‡]Department of Radiology, Duke University Medical Center, Durham, North Carolina

[†]School of Information Science and Engineering, Shandong University, Jinan, Shandong, China

Abstract

Purpose—To evaluate the relationship between liver tumor motion and diaphragm motion.

Methods and Materials—Fourteen patients with hepatocellular carcinoma (10 of 14) or liver metastases (4 of 14) undergoing radiation therapy were included in this study. All patients underwent single-slice cine–magnetic resonance imaging simulations across the center of the tumor in 3 orthogonal planes. Tumor and diaphragm motion trajectories in the superior–inferior (SI), anterior–posterior (AP), and medial–lateral (ML) directions were obtained using an in-house-developed normalized cross-correlation–based tracking technique. Agreement between the tumor and diaphragm motion was assessed by calculating phase difference percentage, intraclass correlation coefficient, and Bland-Altman analysis (*Diff*). The distance between the tumor and tracked diaphragm area was analyzed to understand its impact on the correlation between the 2 motions.

Results—Of all patients, the mean (±standard deviation) phase difference percentage values were 7.1% ± 1.1%, 4.5% ± 0.5%, and 17.5% ± 4.5% in the SI, AP, and ML directions, respectively. The mean intraclass correlation coefficient values were 0.98 ± 0.02, 0.97 ± 0.02, and 0.08 ± 0.06 in the SI, AP, and ML directions, respectively. The mean *Diff* values were 2.8 ± 1.4 mm, 2.4 ± 1.1 mm, and 2.2 ± 0.5 mm in the SI, AP, and ML directions, respectively. Tumor and diaphragm motions had high concordance when the distance between the tumor and tracked diaphragm area was small.

Conclusions—This study showed that liver tumor motion had good correlation with diaphragm motion in the SI and AP directions, indicating diaphragm motion in the SI and AP directions could potentially be used as a reliable surrogate for liver tumor motion.

Reprint requests to: Fang-Fang Yin, PhD, Department of Radiation Oncology, Duke University Medical Center, Box 3295, Durham, NC 27710. Tel: (919) 660-2185; fangfang.yin@duke.edu.

Conflict of interest: J.Y. received personal fees from the China Scholarship Council during the conduct of the study; J.C. received grants from the National Institutes of Health and the Golfers Against Cancer Foundation during the conduct of the study; H.W. received research grants from the Natural Science Foundation of Shandong Province during the conduct of the study; M.R.B. received grants and personal fees from Siemens Healthcare and Bayer Healthcare, outside the submitted work; Fang-Fang Yin received grants from the National Institutes of Health during the conduct of the study.

Introduction

Respiration-induced organ motion poses a significant challenge to radiation therapy, potentially leading to underdosing the target volume and overdosing the surrounding normal tissues (1). Liver tumor motion is highly impacted by respiration, with the largest induced motion usually observed in the superior–inferior (SI) direction, ranging from 5 to 50 mm (2–4). Recently, many techniques have been implemented to address respiration-induced treatment uncertainties, including adding a safety margin around the target, utilizing voluntary or passive breath-hold, or applying on-board target tracking to enable gated treatment (5–10). To apply these methods effectively, it is critical to accurately monitor target motion trajectories during treatment simulation, setup, and delivery.

The diaphragm, a typical surrogate for liver motion, is often tracked given its visibility on x-ray images (11). An early study using animal models with implanted markers at different locations within the liver indicated that the motion magnitude of the liver varied with the distance between the diaphragm and the measurement point (12). However, few studies are available investigating the correlation between diaphragm motion and liver tumor motion. The feasibility and fidelity of using diaphragm motion as a surrogate for liver tumor motion are unclear.

A number of previous studies have investigated the correlation between 2 organs or tissues (ie, internal and external). Koch et al (13) measured the internal lung motion using the identified lung vessels on magnetic resonance images (MRI) as anatomic landmarks and evaluated the motion correlation between lung and the skin surface. Their results showed that the best correlation was observed between the SI component of lung motion and an abdominal skin surface marker. The strength of the correlation was affected by the locations of the lung vessels and skin markers, as well as the subjects' breathing patterns. Beddar et al (14) investigated the correlation between the motion of an external marker and internal fiducials implanted in the liver for 8 patients undergoing respiratory-based computed tomography (CT). They concluded that the best motion correlation between external respiration and internal fiducials was observed during expiration. Kirlivola et al (11) measured 3-dimensional (3D) motion of liver tumors using T2-weighted cine-MRI and compared with liver motion that was measured using fluoroscopy in 36 liver cancer patients. Diaphragm excursion was used as the surrogate of liver tumor motion for fluoroscopy. Their results confirmed the validity of using cine-MRI to track liver tumor motion in 3 orthogonal directions. However, the liver tumor motion measured on cine-MRI did not correlate well with the diaphragm motion measured on fluoroscopy ($\gamma = 0.25$). The authors indicated that diaphragm motion at these cine-MRI slices did not represent the full or maximal diaphragm motion as assessed using fluoroscopy. Therefore, diaphragm motion was not measured on cine-MRI. The limitation of this approach was that the liver tumor and diaphragm motion trajectories were obtained at differing times, using 2 different imaging protocols. Potential errors might have occurred due to different respiratory patterns between 2 separate acquisitions. An additional limitation of using fluoroscopy to measure the diaphragm motion was that the angle of the beam was not perpendicular to the dome of the diaphragm.

With high soft-tissue contrast and an absence of radiation hazard, MRI is becoming widely utilized in radiation therapy. In addition, fast MRI sequences such as cine-MRI can be used to capture near real-time images of target motion. The successful implementation (15, 16) of cine-MRI to track target motion opens up a new avenue to track diaphragm and liver tumor motion together and address their correlation. In this study we attempt to demonstrate the suitability of using diaphragm motion, which is easily visualized on MRI, as a surrogate for tracking liver tumor motion. Single-slice cine-MRI images in 3 orthogonal planes (SI, anterior–posterior [AP], and medial–lateral [ML]) were used to simultaneously measure both liver tumor and diaphragm motion. An automatic method based on template matching was used to track both diaphragm and liver tumor motion in the SI, AP, and ML directions. Once liver tumor and diaphragm motion were extracted from the MRIs in 3 orthogonal directions, the reliability of diaphragm as a surrogate was tested by comparing the following parameters: phase difference percentage (PDP), intraclass correlation coefficient (ICC), and Bland-Altman analysis (*Diff*). We also evaluated the correlation of the distance (*D*) between the tumor and the tracked diaphragm area with respect to their motion.

Methods and Materials

Patient cohort and imaging study

Fourteen cancer patients (7 male, 7 female; mean age 61 years) with hepatocellular carcinoma (10 of 14) or liver metastases (4 of 14) were enrolled in this study. Eight patients received MR scans under an institutional review board–approved protocol with informed consent, and 6 as part of clinical imaging. Institutional review board approval was obtained to retrospectively collect patient images, and the requirement for informed consent was waived. Table 1 summarizes the clinical characteristics of the patients.

All MR scans were acquired on a 1.5-Tesla (Signa; GE Healthcare, Milwaukee, WI) or a 3.0-Tesla (MAGNETOM Trio; Siemens Medical Systems, Erlangen Germany) MR system. For each patient, single-slice cine-MRI images were acquired through the center of the liver tumor in axial, coronal, and sagittal views using a fast steady-state acquisition protocol labeled as FIESTA by GE (17, 18) and TrueFISP by Siemens (19, 20), with either a 6- or a 12-channel phased-array coil. The scanning time was set to approximately 15 to 30 seconds for each imaging view. All patients were positioned head-first-supine in an immobilization device during image acquisition. The MRI parameters were optimized to achieve fast imaging speed and to maintain adequate spatial resolution with the following parameter settings: temporal resolution: 6 frames per second; repetition time/echo time: 2.56 ms/0.83 ms; flip angle: 50°; bandwidth: 976.562 Hz per pixel; field of view: 360 mm × 240 mm; slice thickness: 5 mm; slice dimension: 192 × 128; and in-plane slice resolution: 1.875 mm × 1.875 mm.

Motion tracking technique based on normalized cross-correlation

Given that only the 2-dimensional (2D) in-plane motion can be tracked from single-slice cine-MRI images, to track the motion trajectories of the diaphragm and liver tumor on the acquired cine-MRI images, an in-house-developed tracking technique based on normalized cross-correlation (NCC) was used (21). The NCC method maximizes the NCC coefficient

through moving and matching a manually selected feature-based imaging template along fixed background images. The boundaries of the diaphragm in the cine-MRI images of each patient were easily distinguished in our study, and the reliability of detecting the diaphragm was ensured. The imaging template was selected on the diaphragm (for diaphragm tracking) or the liver tumor (for liver tumor tracking) from the first acquired cine-MRI image. The imaging template of the diaphragm in coronal and sagittal views was placed on the dome of the diaphragm for each patient (Fig. 1). The fixed background images were the later sequentially acquired cine-MRI images. The coefficient R between the imaging template (A_1) and the corresponding area (A_2) on each fixed background image was calculated using Eq. 1, where $var(A_1)$ and $var(A_2)$ represent the variances of A_1 and A_2, and $cov(A_1, A_2)$ is the covariance of A_1 and A_2. The motion of the diaphragm or tumor, represented by the shifts of A_1, was determined by the difference between the location of the best-matched A_2 (Eq. 2) on each fixed background image and the nominal location of A_1 on the first acquired cine-MRI image (Fig. 2). The motion trajectory of the diaphragm or the liver tumor was built by concatenating the sequential shifts of A_1.

$$R(A_1, A_2) = \frac{cov(A_1, A_2)}{(var(A_1)var(A_2))^{1/2}} \quad (1)$$

$$A_2 = argmax(R(A_1, A_2)) \quad (2)$$

The double estimate of axis-specific motion was included in this study, because the acquired data provided a double estimate of the motion characteristics along the SI, AP, and ML directions. For example, the AP motion could be extracted from the sagittal and axial planes with cross-plane motion in ML and SI directions, respectively. By comparing the ML motion extracted from the coronal and axial planes and the SI motion extracted from the sagittal and coronal planes, we found that the SI motion was much larger than the ML motion. We therefore chose the AP motion information extracted from the sagittal plane because the cross-plane (ie, ML) motion in the sagittal plane was of less concern. The motion trajectory in the SI or ML direction was extracted from the sagittal or coronal plane owing to concerns about errors caused by the cross-plane (ie, AP or SI) motion in either the coronal or axial plane. The tracked motion trajectories from the coronal and sagittal views were combined to measure the diaphragm and liver tumor motion in 3 dimensions. Although our intention was to use the same template in each tracking process, the base template was manually drawn and could be slightly different between different tracking processes. To minimize tracking errors due to human variation in template selection, the tracking was repeated 5 times. The use of repeated measurements to determine average tumor and diaphragm motion trajectories could eliminate this human variation.

Comparison of 3D motion trajectories

For the tumor and diaphragm motion trajectories obtained above, the maximal and average magnitudes, denoted by T_{max}, Dia_{max}, T_{ave}, and Dia_{ave}, were determined for comparison.

The average period (T_{Ave_D}) of each diaphragm motion trajectory was calculated by averaging lengths of all breathing cycles. Phase difference percentage was calculated as the mean difference between the time indices corresponding to the diaphragm motion peaks (T_{Peak_D}) and the time indices corresponding to the tumor motion peaks (T_{Peak_T}) normalized by the T_{Ave_D}, indicating the phase difference between the 2 motions (Eq. 3).

$$PDP = \left(\overline{T_{Peak\_D} - T_{Peak\_T}}\right) / T_{Ave\_D} \quad (3)$$

ICC with 95% confidence intervals (CIs) were calculated to evaluate the trend of the tumor and diaphragm motion trajectories, using the commercial software package SPSS (version 19.0; IBM, Chicago, IL). The ICC operates on data structured as groups, rather than data structured as paired observations, prohibiting outliers in the data groups from influencing the total correlation measured (22).

However, ICC values alone are not sufficient to conclude a good relationship between the liver tumor and diaphragm motion, because they only indicate the level of similarity in the trend change between the 2 motion trajectories, rather than providing a point-by-point comparison. For example, liver tumor motion and diaphragm motion might be very different even if they had a high ICC value. The Bland-Altman analysis was a complementary measurement metric to better evaluate their relationship by comparing the differences of magnitudes between the 2 motions. The difference of magnitudes (*Diff*) was calculated between the 2 on a patient-by-patient basis. The mean difference ($\overline{Diff}$) for all patients was then calculated by averaging those *Diff* values, indicating a tendency of agreement. The random bias was calculated as the standard deviation (SD) of the *Diff* values, indicating the dispersion degree of those differences. Finally, the 95% CI was constructed according to Eq. 4:

$$95\%CI = \overline{Diff} \pm 1.96 * SD \quad (4)$$

To investigate what factors might affect the correlation between the liver and diaphragm motion, we also measured the distance between the tumor center and the tracked diaphragm area center, denoted by *D*, and studied the relationship between correlation (defined as ICC and *Diff*) and *D* in 3 orthogonal directions (SI, AP, and ML) in all patients. The parameter *D* was measured as the distance from the tumor center to the tracked diaphragm area, following an SI line on either sagittal or coronal MR images (Fig. 1). Evaluation of relationship was accomplished by plotting the ICC or *Diff* values relative to the corresponding *D* values for all patients, and then fitting those points to a curve using a quadratic polynomial formula. From the trend of the fitted curve, we were able to find the relationship between correlation and *D*.

Results

Figure 3 shows the comparison of liver tumor and diaphragm motion in the SI, AP, and ML directions for patient 1. Figure 4 shows the Bland-Altman plot illustrating the difference between the 2 types of motion for all patients.

The mean T_{max} values were 16.5 mm (range, 4.5–24.6 mm), 10.6 mm (range, 6.8–15.0 mm), and 3.4 mm (range, 1.8–4.0 mm) in the SI, AP, and ML directions, respectively. In comparison, the mean Dia_{max} values were 16.6 mm (range, 4.0–25.1 mm), 10.2 mm (range, 7.4–15.2 mm), and 4.4 mm (range, 2.1–6.9 mm) in the SI, AP, and ML directions, respectively. The mean T_{ave} values were 15.2 mm (range, 10.4–18.6 mm), 7.5 mm (range, 3.7–11.6 mm), and 0.6 mm (range, 0.6–1.3 mm) in the SI, AP, and ML directions, respectively. In comparison, the mean Dia_{ave} values were 15.7 mm (range, 10.8–19.0 mm), 7.7 mm (range, 3.8–15.8 mm), and 1.6 mm (range, 0.5–2.0 mm) in the SI, AP, and ML directions, respectively. For both liver tumor and diaphragm motion, motions along the SI and AP directions were much larger than those along the ML direction.

Table 1 summarizes the results of all patients. On average, the motion trajectories between tumor and diaphragm matched well in the SI and AP directions, and correlated poorly in the ML direction: the mean (±SD) PDP values were 4.5% ± 0.5%, 7.1% ± 1.1%, and 17.5% ± 4.5% in the SI, AP, and ML directions, respectively; the mean values of ICC were 0.98 ± 0.02, 0.97 ± 0.02, and 0.08 ± 0.06 in the SI, AP, and ML directions, respectively; and the mean values of *Diff* were 2.8 ± 1.4 mm, 2.4 ± 1.1 mm, and 2.2 ± 0.5 mm in the SI, AP, and ML directions, respectively.

Figure 5 shows the relationship between correlation and *D* in 3 orthogonal directions (SI, AP, and ML). The triangles and dots represent the ICC values and the *Diff* values relative to the corresponding *D* values, respectively. The solid and dashed curves were determined by fitting all the ICC values and the *Diff* values using a quadratic polynomial curve in each direction. Observations show that the ICC values decreased with an increase of *D* values, and the *Diff* values increased with an increase of *D* values, in 3 orthogonal directions. The smaller the distance between the tumor and the tracked diaphragm area, the better their correlation.

Discussion

Tumor motion management has been recognized as one of the most significant tasks in treating dynamic tumors, especially for advanced treatment techniques such as proton therapy and intersity modulated radiation therapy, in which precise tumor localization and immobilization are required (23). Effective reduction of radiation margins can be achieved through breath-hold or respiratory gating, both of which require consistent correlation between the tumor location and surrogates of monitoring respiratory, such as skin surface position, diaphragm, or others. In this study, we developed a MRI-based technique to assess liver tumor motion and its relationship to diaphragm motion. Our primary goals were to understand how the liver tumor moves during respiration in liver cancer patients, whether diaphragm can be used as a reliable surrogate to predict such motion, and how the distance

between the tumor and the tracked diaphragm affects their correlation. We not only confirmed the observations regarding liver motion by Yin et al (12) but also systematically analyzed the correlation between liver tumor and diaphragm motion in 3 orthogonal directions (SI, AP, and ML).

Although this new approach is an improvement over fluoroscopy, a limitation of this study lies in the suboptimal tumor-to-tissue contrast-to-noise ratio (CNR) of the FIESTA/TrueFISP sequence with T2*/T1 weighting. Compared with T2-weighted MR images, the T2*/T1 weighting provides inferior tumor-to-tissue CNR. In addition, during image acquisition, artifacts often occur owing to the presence of resonance frequency offsets, originating from suboptimal synthesizer frequency settings (23). Ghost artifacts may also degrade image quality (24). The existence of these artifacts in critical areas, including tumor and normal tissue, hampers accurate tumor and organ delineation, which in turn affects motion tracking accuracy. In this study, imaging parameters of the FIESTA/TrueFISP sequence were carefully adjusted to mitigate the previously mentioned artifacts as much as possible. In addition, MR image distortion is a relevant concern. However, studies have shown that the MR distortion is less than 1 mm within 15-cm radius (25). Because the tracked tumors or diaphragm areas are usually at the center of the MR images, MR distortion is expected to be minimal.

Another limitation of this study is that both liver tumor motion and diaphragm motion were measured as a combination from two 2D views (coronal and sagittal) and not directly from a 3D volumetric image. For large and irregularly shaped tumors, respiration-induced rotations and deformations may render the 2D–2D method inaccurate, given that a single slice may not reflect the motion of the entire tumor volume and that the cross-plane tumor motion can result in a different motion profile of a tumoral edge. The liver tumor motion in the SI direction was not significantly different whether it was extracted from the coronal plane or from the sagittal plane. However, it might be more sensible to extract the SI motion from the sagittal plane because the through-plane motion (ie, ML) was uniformly small.

Potential errors may also occur in the motion trajectories owing to the limitation of the tracking algorithm used. The tracking resolution in the algorithm corresponds to the slice pixel resolution, which cannot detect motion displacement smaller than 1 slice pixel size. Because the tumor motion in the ML direction is small in magnitude, potential errors may occur in tracking results along this direction. Advanced tracking algorithms with better interpolation models will be helpful in future studies. Nevertheless this is currently a lesser concern, given that only diaphragm motion in the SI direction is to serve as a breathing surrogate.

A final limitation is that this pilot study included a limited number of patients. When using the quadratic polynomial curves to fit the ICC or *Diff* values corresponding to different *D* values between tumor and tracked diaphragm, a larger pool of patients is needed to better define the trend of these 2 curves.

Conclusions

Our results showed good correlation between liver tumor motion and diaphragm motion in the SI and AP directions. This implies that diaphragm motion in the SI and AP directions could be a potentially reliable surrogate for predicting liver tumor motion. Although diaphragm motion was poorly correlated with liver tumor motion in the ML direction, the small magnitude of liver tumor motion in that direction suggested that it might be clinically irrelevant.

Acknowledgments

This work is partly supported by research grants from the National Institutes of Health (1R21CA165384-01A1) and the Golfers Against Cancer Foundation, as well as by an educational fund from the China Scholarship Council.

The authors thank Mr You Zhang from the Department of Radiation Oncology, Duke University Medical Center, for the revision of the manuscript.

References

1. Lambert J, Suchowerska N, Mckenzie DR, et al. Intrafractional motion during proton beam scanning. Phys Med Biol. 2005; 50:4853–4862. [PubMed: 16204877]
2. Davies SC, Hill AL, Holmes RB, et al. Ultrasound quantitation of respiratory organ motion in the upper abdomen. Br J Radiol. 1994; 67:1096–1102. [PubMed: 7820402]
3. Balter JM, Dawson LA, Kazanjian S, et al. Determination of ventilatory liver movement via radiographic evaluation of diaphragm position. Int J Radiat Oncol Biol Phys. 2001; 51:267–270. [PubMed: 11516877]
4. Suramo I, Paivansalo M, Myllyla V. Cranio-caudal movements of the liver, pancreas and kidneys in respiration. Acta Radiol Diagn. 1984; 25:129–131.
5. Keall PJ, Mageras GS, Balter JM, et al. The management of respiratory motion in radiation oncology report of AAPM Task Group 76. Med Phys. 2006; 33:3874–3900. [PubMed: 17089851]
6. Webb S. Motion effects in (intensity modulated) radiation therapy: A review. Phys Med Biol. 2006; 51:R403–R425. [PubMed: 16790915]
7. Torizuka T, Tanizaki Y, Kanno T, et al. Single 20-second acquisition of deep-inspiration breath-hold PET/CT: Clinical feasibility for lung cancer. J Nucl Med. 2009; 50:1579–1584. [PubMed: 19759111]
8. Onishi H, Kuriyama K, Komiyama T, et al. Clinical outcomes of stereotactic radiotherapy for stage I non-small cell lung cancer using a novel irradiation technique: Patient self-controlled breath-hold and beam switching using a combination of linear accelerator and CT scanner. Lung Cancer. 2004; 45:45–55. [PubMed: 15196734]
9. Murphy MJ, Martin D, Whyte R, et al. The effectiveness of breath-holding to stabilize lung and pancreas tumors during radio-surgery. Int J Radiat Oncol Biol Phys. 2002; 53:475–482. [PubMed: 12023152]
10. Nelson C, Starkschall G, Balter P, et al. Respiration-correlated treatment delivery using feedback-guided breath-hold: A technical study. Med Phys. 2005; 32:175–181. [PubMed: 15719968]
11. Kirilova A, Lockwood G, Choi P, et al. Three-dimensional motion of liver tumors using cine-magnetic resonance imaging. Int J Radiat Oncol Biol Phys. 2008; 71:1189–1195. [PubMed: 18258378]
12. Yin F, Kim JG, Haughton C, et al. Extracranial radiosurgery: Immobilizing liver motion in dogs using high-frequency jet ventilation and total intravenous anesthesia. Int J Radiat Oncol Biol Phys. 2001; 49:211–216. [PubMed: 11163517]
13. Koch N, Liu HH, Starkschall, et al. Evaluation of internal lung motion for respiratory-gated radiotherapy using MRI: Part I—correlating internal lung motion with skin fiducial motion. Int J Radiat Oncol Biol Phys. 2004; 60:1459–1472. [PubMed: 15590177]

14. Beddar AS, Kainz K, Briere TM, et al. Correlation between internal fiducial tumor motion and external marker motion for liver tumors imaged with 4D-CT. Int J Radiat Oncol Biol Phys. 2007; 67:630–638. [PubMed: 17236980]
15. Cervino LI, Du J, Jiang SB. MRI-guided tumor tracking in lung cancer radiotherapy. Phys Med Biol. 2011; 56:3773–3785. [PubMed: 21628775]
16. Michel JG, Jaffray DA, Siewerdsen JH, et al. Prostate gland motion assessed with cine-magnetic resonance imaging (cine-MRI). Int J Radiat Oncol Biol Phys. 2005; 62:406–417. [PubMed: 15890582]
17. Scheffler K, Lehnhardt S. Principle and applications of balanced SSFP techniques. Eur Radiol. 2003; 13:2409–2418. [PubMed: 12928954]
18. Ayman J, Oweida MS, Elizabeth A, et al. Iron-oxide labeling of hematogenous macrophages in a model of experimental autoimmune encephalomyelitis and the contribution to signal loss in fast imaging employing steady state acquisition (FIESTA) images. J Magn Reson Imaging. 2007; 26:144–151. [PubMed: 17659552]
19. Herborn CU, Vogt F, Lauenstein TC, et al. MRI of the liver: Can true FISP replace HASTE? J Magn Reson Imaging. 2003; 17:190–196. [PubMed: 12541226]
20. Scheffler K, Hennig J. T_1 quantification with inversion recovery TrueFISP. Magn Reson Med. 2001; 45:720–723. [PubMed: 11284003]
21. Cai J, Sheng K, Sheehan JP, et al. Evaluation of thoracic spinal cord motion using ynamic MRI. Radiother Oncol. 2007; 84:279–282. [PubMed: 17692979]
22. Weir JP. Quantifying test-retest reliability using the intraclass correlation coefficient and the SEM. J Strength Cond Res. 2005; 19:231–240. [PubMed: 15705040]
23. Torres M, Onodera Y, Bengua G, et al. Outcome and pneumonitis in lung cancer patients treated with stereotactic real-time tumor-tracking radiotherapy. Int J Radiat Oncol Biol Phys. 2009; 75:457–458.
24. Cai J, Chang Z, Wang Z, et al. Four-dimensional magnetic resonance imaging (4D-MRI) using image-based respiratory surrogate: A feasibility study. Med Phys. 2011; 38:6384–6394. [PubMed: 22149822]
25. Chen Z, Ma CM, Paskalev K, et al. Investigation of MR image dostortion for radiotherapy treatment planning of prostate cancer. Phys Med Biol. 2006; 52:1393–1404. [PubMed: 16510951]

Summary

This study aims to investigate the relationship between liver tumor motion and diaphragm motion by comparing their motion trajectories obtained from cine–magnetic resonance imaging. This study showed that liver tumor motion had good correlation with diaphragm motion in the superior–inferior and anterior–posterior directions. Tumor and diaphragmatic motion had high concordance when the distance between the tumor and tracked diaphragm area was small.

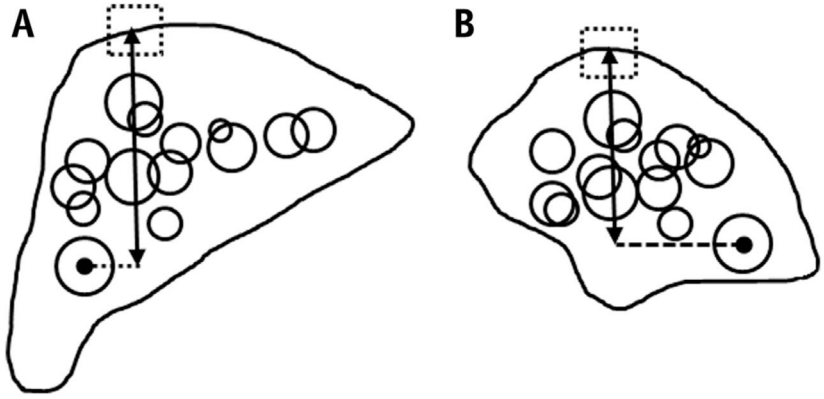

Fig. 1.

Coronal (a) and sagittal (b) views of tumors (circles) from all patients and one sample tracked diaphragm area (dashed squares). The measured distance between tumor and tracked diaphragm area was indicated by the superior–inferior line with the arrows on both ends.

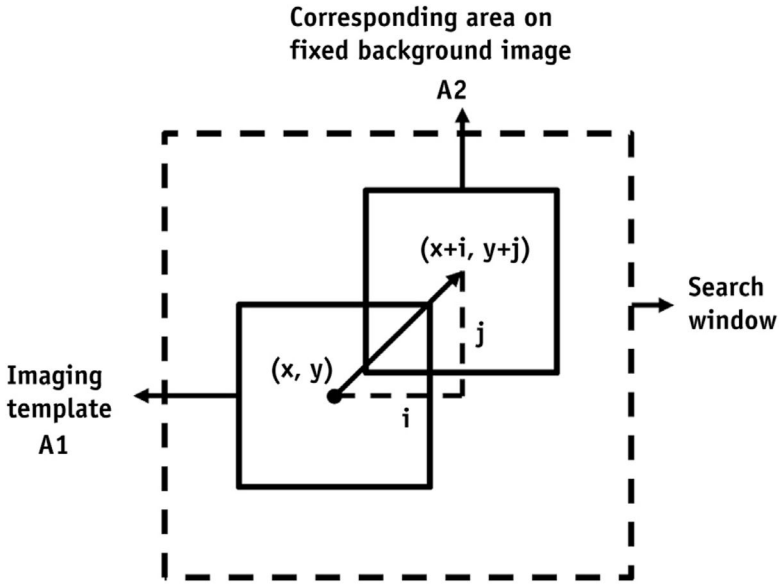

Fig. 2.

The normalized cross-correlation method was used for motion tracking. Point (x, y) was located at the center of the imaging template A_1, and point $(x + i, y + j)$ was the corresponding point in the fixed background image A_2. Vector (i, j) reflected the shift of A_1. The search window was defined to confine the range of each tracking.

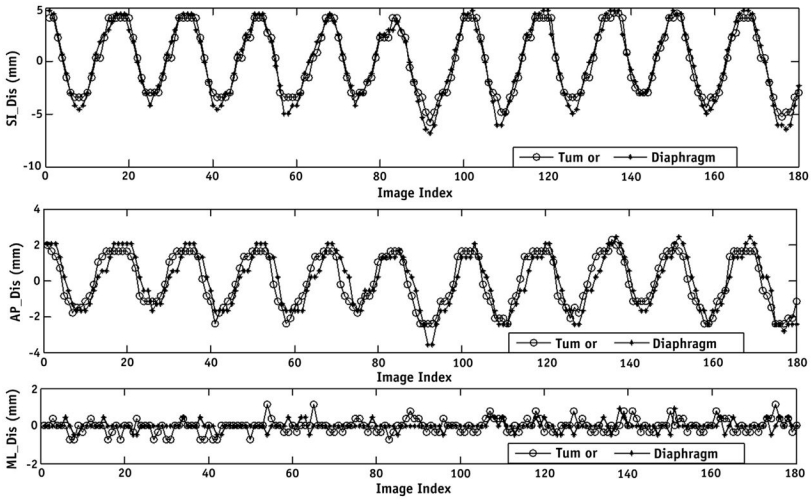

Fig. 3.

Comparison of liver tumor and diaphragm motion trajectories determined by using the tracking technique based on normalized cross-correlation in 3 orthogonal directions (superior–inferior [SI], anterior–posterior [AP], and medial–lateral [ML]) for patient 1.

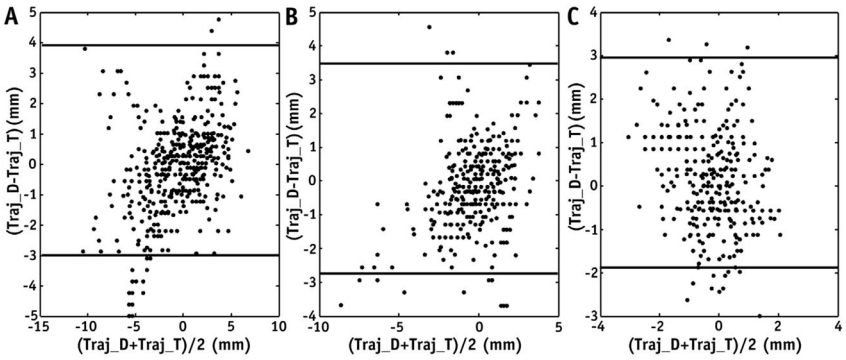

Fig. 4.

Scatter plots showing the results of Bland-Altman analysis for liver tumor and diaphragm motion trajectories in the superior–inferior (A), anterior–posterior (B), and medial–lateral (C) directions for all patients. The circles represent the difference values of the magnitudes (*Traj_D − Traj_T*) between diaphragm motion (*Traj_D*) and tumor motion (*Traj_T*). The solid lines represent the top and bottom 95% confidence interval values.

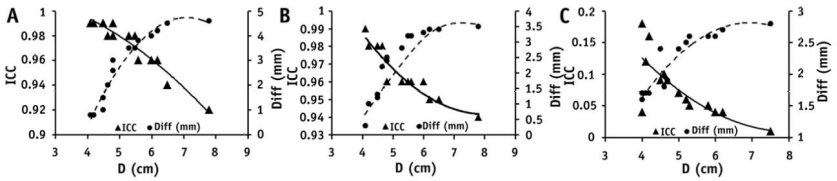

Fig. 5.

The relationship between correlation (defined as intraclass correlation coefficient [ICC] or *Diff*) and distance (*D*) between liver tumor and tracked diaphragm area in the superior–inferior (A), anterior–posterior (B), and medial–lateral (C) directions in all patients. The triangles and dots represent the ICC values and the *Diff* values relative to corresponding *D* values, respectively. The solid and dashed curves were determined by fitting the ICC values and the *Diff* values using a quadratic polynomial formula in each direction.

Table 1

Summary of patient characteristics and measurements between diaphragm motion and liver tumor motion evaluated by PDP, ICC, and Bland-Altman analysis from all patient subjects

				PDP (%)			ICC						Bland-Altman analysis					
							SI		AP		ML		SI		AP		ML	
Patient	Age (y)	Sex	Cancer site	SI	AP	ML	ICC	95% CI	ICC	95% CI	ICC	95% CI	*Diff* (mm)	95% CI	*Diff* (mm)	95% CI	*Diff* (mm)	95% CI
1	70	M	HCC	6.5	4.5	20.5	0.99	0.98–0.99	0.99	0.93–0.96	0.18	−0.28–0.29	0.8	−1.46–1.46	0.3	−1.29–1.29	1.6	−0.87–0.87
2	68	F	HCC	6.8	4.8	15.2	0.98	0.97–0.99	0.98	0.95–0.98	0.1	−0.20–0.35	2.0	−1.68–1.75	2.2	−1.28–1.32	1.8	−0.56–0.55
3	67	F	HCC	6.0	5.2	15.0	0.96	0.96–0.99	0.95	0.95–0.99	0.04	−0.26–0.30	4.2	−1.52–1.55	3.4	−1.30–1.30	2.6	−0.88–0.78
4	34	F	HCC	7.0	4.9	25.6	0.98	0.96–1.00	0.96	0.98–0.99	0.06	−0.40–0.45	3.5	−1.50–1.80	3.2	−1.22–1.50	2.5	−0.85–0.79
5	68	F	HCC	6.5	4.0	15.8	0.96	0.98–1.00	0.96	0.98–1.00	0.05	−0.22–0.28	3.8	−1.34–1.42	3.2	−1.28–1.24	2.6	−0.77–0.69
6	67	M	Liver Mets	8.0	5.5	16.0	0.94	0.93–0.98	0.95	0.96–0.98	0.04	−0.24–0.28	4.5	−1.42–1.45	3.4	−1.26–1.26	2.7	−0.82–1.05
7	55	M	HCC	6.0	3.2	24.5	0.96	0.99–1.00	0.96	0.94–0.97	0.05	−0.35–0.48	4.0	−1.38–1.47	3.3	−1.26–1.25	2.6	−0.90–1.14
8	54	M	HCC	6.5	4.7	21.5	0.98	0.92–0.99	0.96	0.95–0.96	0.09	−0.52–0.54	2.6	−1.35–1.49	2.4	−1.27–1.27	1.9	−0.88–1.00
9	60	F	HCC	7.6	4.9	18.5	0.99	0.95–0.99	0.98	0.95–0.97	0.12	−0.40–0.65	1.5	−1.42–1.46	1.3	−1.30–1.27	1.7	−0.79–0.92
10	73	M	HCC	7.0	5.0	17.0	0.99	0.95–0.99	0.98	0.96–0.98	0.04	−0.21–0.30	1.0	−1.54–1.80	1.2	−1.32–1.26	1.7	−0.54–0.65
11	22	M	Liver Mets	8.8	4.3	13.4	0.99	0.98–1.00	0.98	0.97–0.99	0.16	−0.65–0.85	0.8	−2.90–2.90	1	−3.20–3.20	1.7	−2.50–2.50
12	55	F	Liver Mets	6.2	4.2	12.0	0.98	0.98–1.00	0.96	0.92–0.95	0.07	−0.52–0.50	3.5	−1.84–1.72	2.8	−1.20–1.22	2.4	−0.79–0.82
13	62	M	Liver Mets	5.4	4.0	10.5	0.92	0.99–1.00	0.94	0.99–1.00	0.01	−0.38–0.20	4.6	−1.30–1.40	3.5	−1.24–1.20	2.8	−0.80–1.04
14	75	F	HCC	7.2	4.5	20.1	0.99	0.95–0.99	0.96	0.98–0.99	0.09	−0.43–0.35	3.0	−1.34–1.43	2.5	−1.25–1.30	2.4	−0.72–0.65
Mean	61	—	—	7.1	4.5	17.5	0.98	—	0.97	—	0.08	—	2.8	—	2.4	—	2.2	—
SD	15	—	—	1.1	0.5	4.5	0.02	—	0.02	—	0.06	—	1.4	—	1.1	—	0.5	—

Abbreviations: AP = anterior–posterior; CI = confidence interval; *Diff* = difference in motion amplitude; F = female; HCC = hepatocellular carcinoma; ICC = intraclass coefficient correlation; Liver Mets = liver metastasis; M = male; ML = medial–lateral; PDP = phase difference percentage; SD = standard deviation; SI = superior–inferior.